

## Satellite Encounters

J.-M. PETIT AND M. HENON\*

*Observatoire de Nice, B.P. 139, 06003 Nice Cedex, France, and \*Centre National de la Recherche Scientifique*

Received October 21, 1985; revised February 3, 1986

We study numerically the interaction of two small satellites, initially on circular orbits with slightly different radii. We show first that by going to Hill's limit of vanishing masses, one can reduce the problem to a simpler form in which only one dimensionless parameter remains: the reduced impact parameter. We present then a detailed study of the family obtained when this parameter is varied. Each orbit consists of three phases: approach of the two small bodies, interplay, and departure. Fourth-order series are used to represent the asymptotic motion of the two small bodies in the approach and departure phases; these series are matched with a numerical integration of the interplay phase to give an accurate representation of the entire orbit. For each orbit, we compute the net effect of the encounter, essentially characterized by an increase of the separation of the satellite orbits. We compute also the minimal distance of approach of the two satellites. In the limiting cases of large and small impact parameters, the results are compared with the predictions of perturbation theories. Finally we study the "transitions," which are apparent discontinuities of the family with a sudden change of the direction of departure. We show that they can be explained by the asymptotic approach of the orbit to an unstable periodic solution of Hill's problem. Transitions take place for infinitely many values of the parameter, forming a Cantor-like set. © 1986 Academic Press, Inc.

### 1. INTRODUCTION

We consider the following problem. Two light bodies  $M_2$  and  $M_3$  describe initially coplanar and circular orbits, with slightly different radii, around a heavy central body  $M_1$ . Bodies  $M_2$  and  $M_3$  are initially far apart, so that their mutual attraction is negligible. However, the inner body has a slightly larger angular velocity and eventually catches up with the outer body; the distance from  $M_2$  to  $M_3$  becomes small and their mutual attraction is no longer negligible. We shall call this an *encounter*. (An encounter should not be confused with a physical *collision* between the two bodies.) What is the motion of  $M_2$  and  $M_3$  during and after the encounter?

This problem covers a number of actual situations in astronomy; in particular, the gravitational interaction between particles in planetary rings, with incidences on the ring radial structure (Goldreich and Tremaine, 1979, 1980; Hénon, 1981, 1984) and

on the azimuthal brightness variation (Franklin and Colombo, 1978; Karttunen, 1983); the motion of coorbital satellites, such as Saturn's Janus and Epimetheus satellites (Dermott and Murray, 1981; Yoder *et al.*, 1983); the accretion of particles by a proto-planet (Schofield, 1981) with incidences on its rate of rotation (Giuli, 1968a,b); the distribution of particles around the Earth (Dole, 1962).

For convenience,  $M_1$  will be called the *planet* and  $M_2$ ,  $M_3$  will be called the *satellites*. However, the model is applicable to more general situations. For instance,  $M_1$  can be the Sun while  $M_2$  and  $M_3$  are planets or interplanetary particles, as in the last two items of the above list. The difference between the radii of the initial circular orbits will be called the *impact parameter*.

A number of equations and analytical developments will be needed. They are described in a companion paper (Hénon and Petit, 1986), which will be referred to as Paper I.

The problem is a particular case of the general three-body problem. Analytic approximations of the solution are available in two cases:

(i) When the impact parameter is sufficiently large, the result of the encounter is only a slight deflection of  $M_2$  and  $M_3$  from their previous circular orbits. These deflections can then be obtained by a perturbation theory (Goldreich and Tremaine, 1979, 1980).

(ii) When the impact parameter is very small, the interaction of  $M_2$  and  $M_3$  produces a "horseshoe" motion:  $M_2$  and  $M_3$  "repel" each other azimuthally and never come in close proximity. This case can also be treated by a perturbation theory (Dermott and Murray, 1981; Yoder *et al.*, 1983).

Between these two asymptotic cases, however, no theory exists, and apparently only a numerical integration of the equations of motion can give the answer. Indeed, the computed orbits are sometimes so complicated (see Fig. 1) that it seems doubtful that a theory will ever be able to account for them.

In the present paper, we shall explore the problem by means of numerical integration, for all values of the impact parameter, so as to bridge the gap between the two above approximations. Scattered computations exist already in the literature (Dole, 1962; Giuli, 1968a; Franklin and Colombo, 1978; Dermott and Murray, 1981; Schofield, 1981; Karttunen, 1983), but no systematic, detailed exploration of the problem appears to have been made. Our first aim is to produce basic reference material for the various applications. However, the family of solutions is also of interest in itself; as will be seen, it has some remarkable properties.

The present work differs from the earlier computations in other important respects. First, these computations used the standard equations of the general three-body problem. After appropriate choices of units, the problem then still contains three essential

parameters: the ratio of the two initial orbit radii, and the ratios of the masses of the two satellites to the mass of the planet. A detailed exploration of this three-dimensional parameter space is not feasible. We shall show, however, that if the masses of the satellites are small compared to the mass of the planet (this is the case in all applications), the equations can be reduced to a simpler form, which is the classical set of Hill's equations. This new form has a number of advantages:

(1) Only one parameter,  $h$ , remains;  $h$  is essentially a reduced impact parameter. We have then to consider only a one-parameter family of orbits, which can be computed and tabulated in as much detail as we wish. With appropriate scale conversions, this single family covers all practical cases of interest.

(2) This new formulation is more natural and much better adapted to numerical computation. The original equations of the three-body problem contain quantities with very different orders of magnitude, and this degrades the accuracy: for instance the distance between the two satellites is computed as a small difference between two large numbers and is therefore ill-determined, yet this distance plays a critical role in the overall accuracy. Numerical computation becomes impossible if the masses of the satellites are too small (Franklin and Colombo, 1978). By contrast, in Hill's equations no small quantity is left; everything is of order unity, and full accuracy is maintained even in the limit of vanishing satellite masses.

(3) Hill's problem has an additional symmetry with respect to the radial coordinate. This halves the number of orbits to be considered. It also explains the quasi-symmetries observed in earlier computations.

(4) Computation is faster since Hill's equations are simpler than the full three-body equations.

We emphasize that, contrary to what is often believed, it is not necessary that one

of the satellites has a small mass compared to the other for Hill's equations to be applicable. Any mass ratio is acceptable (see Paper I).

Another improvement in the present work resides in the computation of the starting values for the numerical integration. In all earlier computations, a zero-order approximation has been used: the starting values are simply those of the circular orbits. Here we use a high-order approximation, obtained by integrating analytically the mutual effect of the two satellites up to the time at which numerical integration is started (see Paper I). Symmetrically, at the end of the numerical integration, the orbit is matched to an asymptotic solution in order to obtain accurate final values.

As this paper was being prepared, we were informed of the existence of recent work on the same subject by Spirig and Waldvogel (1985).

2. EQUATIONS

2.1. Reduction to Hill's Equations

Only a brief review of the reduction to Hill's equations will be given here; details can be found in Paper I. We assume that the mass of either satellite is small compared to the mass of the planet:

$$m_2 \ll m_1, \quad m_3 \ll m_1, \quad (1)$$

where  $m_i$  is the mass of body  $M_i$ . We assume also that the distance between the two satellites is small compared to their distance to the planet. In a zero-order approximation, the two satellites can then be considered as a single body in orbit around the planet. This orbit will be called the *mean orbit*, and will be assumed to be circular. We call  $a_0$  the radius of the mean orbit. (The precise definition of  $a_0$  does not matter, as long as it is nearly equal to the radii of the satellite orbits). The angular velocity on the mean orbit is

$$\omega = \sqrt{Gma_0^{-3}} \quad (2)$$

where  $m$  is the total mass of the system:

$$m = m_1 + m_2 + m_3. \quad (3)$$

We define

$$\mu = \frac{m_2 + m_3}{m}. \quad (4)$$

Let  $X_i, Y_i$  be the coordinates of body  $i$  in an inertial system. We introduce dimensionless coordinates by

$$X'_i = \frac{X_i}{a_0}, \quad Y'_i = \frac{Y_i}{a_0},$$

$$m'_i = \frac{m_i}{m}, \quad t' = \omega t, \quad (5)$$

and for simplicity we drop the primes in what follows. In the new variables, the radius of the orbit, the angular velocity, the mass of the system, and the gravitational constant are all equal to 1. We choose the origin of time so that the two satellites are in the vicinity of  $X = 1, Y = 0$  at  $t = 0$ . We introduce new coordinates  $\xi, \eta$ , which will be called *Hill's coordinates*:

$$X_i - X_1 = (1 + \mu^{1/3}\xi_i) \cos t - \mu^{1/3}\eta_i \sin t,$$

$$Y_i - Y_1 = (1 + \mu^{1/3}\xi_i) \sin t + \mu^{1/3}\eta_i \cos t.$$

( $i = 2, 3$ ) (6)

We go over to new coordinates  $\xi^*, \eta^*, \xi, \eta$ , describing, respectively, the position of the center of mass and the relative position of the two satellites:

$$\xi^* = \frac{m_2\xi_2 + m_3\xi_3}{m_2 + m_3}, \quad \eta^* = \frac{m_2\eta_2 + m_3\eta_3}{m_2 + m_3},$$

$$\xi = \xi_3 - \xi_2, \quad \eta = \eta_3 - \eta_2. \quad (7)$$

The equations for the motion of the center of mass are linear and easily integrated (Paper I). The equations of relative motion are approximately

$$\ddot{\xi} = 2\ddot{\eta} + 3\xi - \frac{\xi}{\rho^3}, \quad \ddot{\eta} = -2\ddot{\xi} - \frac{\eta}{\rho^3},$$

$$\rho = \sqrt{\xi^2 + \eta^2}, \quad (8)$$

which are *Hill's equations* (Hill, 1878). The error in these equations is of the order of

$\mu^{1/3}$ . They become exact in the limit of vanishing satellite masses. In the case of Saturn's rings, for instance, a typical value for  $\mu$  is  $10^{-24}$ , so that the error in Hill's equations is of the order of  $10^{-8}$ . For the coorbiting satellites Janus and Epimetheus,  $\mu$  is of the order of  $10^{-9}$  and the error is of the order of  $10^{-3}$ .

Hill's equations admit the integral

$$\Gamma = 3\xi^2 + \frac{2}{\rho} - \dot{\xi}^2 - \dot{\eta}^2 \quad (9)$$

which can be called the *Jacobi integral* by analogy with the restricted problem.

Note that Hill's equations are the same for all values of the satellite masses.

### 2.2. Initial Values

We assume that before their encounter, the two satellites are on circular orbits, with radii  $a_2$  and  $a_3$  close to  $a_0$ . We write

$$a_2 = a_0(1 + \mu^{1/3}h_2), \quad a_3 = a_0(1 + \mu^{1/3}h_3). \quad (10)$$

As is easily shown, these circular orbits appear in Hill's coordinates as rectilinear motions

$$\xi_i = h_i, \quad \eta_i = -\frac{3}{2}h_i(t - \tau_i) \quad (i = 2, 3). \quad (11)$$

The constants  $\tau_2, \tau_3$  represent the phases of  $M_2$  and  $M_3$  on their orbits. The relative unperturbed motion is then

$$\xi = h, \quad \eta = -\frac{3}{2}h(t - \tau) \quad (12)$$

with

$$h = h_3 - h_2, \quad \tau = \tau_3 - \tau_2. \quad (13)$$

For a large relative distance, (8) reduces to

$$\ddot{\xi} = 2\dot{\eta} + 3\xi, \quad \ddot{\eta} = -2\dot{\xi}, \quad (14)$$

and it can be verified that (12) is indeed a solution of (14).

The initial motion (12) depends on two parameters  $h$  and  $\tau$ . However,  $\tau$  is a trivial parameter which can be eliminated by a simple change of the origin of time. Therefore the orbits which we are considering

form essentially a one-parameter family, which we shall call *family SE* (for satellite encounter). The parameter  $h$  will be called the *reduced impact parameter*, or the *impact parameter* for short.

Only positive values of  $h$  need to be considered, because of the symmetries of the equations of motion (8): to any solution there corresponds another solution symmetric with respect to the origin. (We can also ensure that  $h$  is positive by defining  $M_2$  as the inner satellite and  $M_3$  as the outer satellite.) We assume therefore

$$h > 0. \quad (15)$$

(We can ignore the case  $h = 0$ : in that case, the two satellites describe the same circular orbit with the same angular velocity and never approach each other.) From (12) we deduce that before the encounter, both  $\xi$  and  $\eta$  are positive: the incoming relative orbit lies in the first quadrant.

Now we consider the full equations (8) and we seek the solution which has the asymptotic form (12) for  $t \rightarrow -\infty$ . Actually our problem is of the singular perturbation type, and it is found (see Paper I) that the asymptotic motion for the perturbed problem has the form

$$\xi = h, \quad \eta = -\frac{3}{2}h(t - \tau) - \frac{1}{3}h^{-2} \ln[-\frac{3}{2}h(t - \tau)], \quad (16)$$

which differs from (12) by the addition of a logarithmic term.

The equations of motion have an inherent time scale of order unity, because the unperturbed equations (14) admit oscillating solutions with frequency 1 (see below). As a consequence, the integration step must always be small compared to unity, even when the satellites are still very far from each other; attempts to use a larger step produce numerical instabilities and inaccurate results. In practice this means that the integration must be started from some finite time  $t_0$ , and that  $|t_0|$  cannot be very large: the time needed to compute the approach of the two satellites is roughly pro-

portional to  $|t_0|$ . Some analytic approximation is therefore required for the solution in the interval  $-\infty < t < t_0$ .

Appropriate expansions have been de-

rived in Paper I. The simplest form of these expansions is obtained by using  $\eta$  as independent variable instead of the time  $t$ . To order 4 in  $\eta^{-1}$ , we have

$$\begin{aligned} \xi &= h - \frac{4}{3}h^{-1}\eta^{-1} - \frac{8}{9}h^{-3}\eta^{-2} + (\frac{17}{3}h - \frac{32}{27}h^{-5})\eta^{-3} + (-\frac{44}{9}h^{-1} - \frac{160}{81}h^{-7})\eta^{-4}, \\ \xi &= -2\eta^{-2} + \frac{5}{2}h^2\eta^{-4}, \\ \dot{\eta} &= -\frac{2}{3}h + 2h^{-1}\eta^{-1} + \frac{4}{3}h^{-3}\eta^{-2} + (-11h + \frac{16}{9}h^{-5})\eta^{-3} + (\frac{32}{3}h^{-1} + \frac{80}{27}h^{-7})\eta^{-4}, \\ t - \tau &= -\frac{2}{3}h^{-1}\eta - \frac{8}{9}h^{-3} \ln \eta + \frac{16}{9}h^{-5}\eta^{-1} + (-\frac{22}{9}h^{-1} + \frac{160}{81}h^{-7})\eta^{-2} \\ &\quad + (-\frac{224}{81}h^{-3} + \frac{2240}{729}h^{-9})\eta^{-3} + (\frac{135}{4}h - \frac{136}{27}h^{-5} + \frac{448}{81}h^{-11})\eta^{-4}. \end{aligned} \tag{17}$$

These series were found to give good accuracy for reasonable values of  $\eta_0$ , the initial value of  $\eta$  corresponding to  $t = t_0$ . Expansions to a higher order could be used (Paper I gives the expansions up to order 8); but this would not necessarily improve the accuracy for a given  $\eta_0$ , because the series (17) are asymptotic and the numerical coefficients increase rapidly with the order. An examination of the series (17) for  $\xi$ ,  $\dot{\xi}$ ,  $\dot{\eta}$  to higher order (see Paper I) shows that the coefficients of  $\eta^{-i}$  for  $i > 0$  involve powers of  $h$  ranging from  $h^{i-2}$  to  $h^{-2i+1}$ . Therefore necessary conditions for these series to give accurate results are

$$h\eta^{-1} \ll 1, \quad h^{-2}\eta^{-1} \ll 1. \tag{18}$$

The value of  $\eta_0$  was accordingly determined by the following formula:

$$\eta_0 = \alpha \max\left(h, \frac{1}{h^2}\right) \tag{19}$$

where  $\alpha$  is a constant whose value depends on the desired accuracy.  $\alpha$  was generally taken equal to 50; the expressions (17) give then the initial values with an accuracy of the order of  $10^{-7}$ . (The accuracy can be estimated simply by comparing numerical integrations of the same orbit started at different values of  $\eta_0$ .)  $\alpha$  was increased to 100 for a few sensitive orbits, for instance in the transition regions (see below).

### 2.3. Final Values

As will be seen in Section 3.1, the two satellites typically interact for a while and

then separate. When they are sufficiently far apart, their mutual attraction becomes again negligible, and each satellite describes a Keplerian orbit around the planet. These orbits are no longer circular, however. In Hill's coordinates, the asymptotic form of the motion is an arbitrary solution of (14), having the general form

$$\begin{aligned} \xi &= h' + k' \cos(t - \varphi'), \\ \eta &= -\frac{2}{3}h'(t - \tau') \\ &\quad - \frac{4}{3}sh'^{-2} \ln[-\frac{2}{3}sh'(t - \tau')] \\ &\quad - 2k' \sin(t - \varphi') \end{aligned} \tag{20}$$

with

$$s = \text{sign}(\eta). \tag{21}$$

This general solution depends on four arbitrary constants  $h'$ ,  $k'$ ,  $\tau'$ ,  $\varphi'$ . (Primes are used to denote final values, corresponding to  $t \rightarrow +\infty$ , while unprimed values such as  $h$  and  $\tau$  in (12) represent initial values, corresponding to  $t \rightarrow -\infty$ .)  $h'$  can be called the impact parameter, as before.  $k'$  is the reduced eccentricity. Note that since the initial motion is circular, the initial value of the reduced eccentricity is  $k = 0$ , while the initial value  $\varphi$  is undefined. The reduced eccentricity  $k'$  is related to the actual eccentricities  $e'_2$ ,  $e'_3$  of  $M_2$  and  $M_3$  by

$$k' = \mu^{-1/3} \sqrt{e_2'^2 + e_3'^2 - 2e_2'e_3' \cos \gamma'} \tag{22}$$

where  $\gamma'$  is the angle between the semimajor axes.

In practice the numerical integration is stopped at some finite time  $t_1$ , when  $|\eta|$  be-

comes again larger than  $\eta_0$  defined by (19), and the values of  $\xi$ ,  $\eta$ ,  $\dot{\xi}$ ,  $\dot{\eta}$  are noted. Here again we need an analytic approximation for the time interval  $t_1 < t < \infty$ , i.e., for matching the end point of the numerical integration to the asymptotic behavior (20). The problem is more difficult since the as-

ymptotic motion has a more general form. The appropriate expansions are derived in Paper I; they are given in terms of an independent variable  $\eta_c$ , which is essentially the averaged value of  $\eta$  over short-period oscillations. To order 4 in  $\eta_c^{-1}$ , these expansions are

$$\begin{aligned} \xi = & h' + k' \cos \theta - \frac{4}{3}sh'^{-1}\eta_c^{-1} + (-\frac{8}{3}h'^{-3} + \frac{7}{6}sh'^{-1}k' \sin \theta)\eta_c^{-2} \\ & + (\frac{17}{3}sh' - \frac{32}{27}sh'^{-5} - \frac{7}{3}sh'^{-1}k'^2 + \frac{23}{4}sk' \cos \theta + \frac{22}{3}h'^{-3}k' \sin \theta)\eta_c^{-3} \\ & + [-\frac{44}{9}h'^{-1} - \frac{160}{81}h'^{-7} - \frac{14}{9}h'^{-3}k'^2 - \frac{42}{12}h'^{-2}k' \cos \theta \\ & + s(-\frac{473}{18}h'k' + \frac{14}{9}h'^{-5}k' + \frac{92}{3}h'^{-1}k'^3) \sin \theta - \frac{5}{3}sk'^2 \sin 2\theta]\eta_c^{-4} + O(\eta_c^{-5}), \end{aligned} \quad (23a)$$

$$\begin{aligned} \eta = & \eta_c - 2k' \sin \theta + (\frac{7}{6}sh'^{-2}k'^2 + \frac{7}{3}sh'^{-1}k' \cos \theta)\eta_c^{-2} \\ & + (\frac{14}{9}h'^{-4}k'^2 + \frac{56}{27}h'^{-3}k' \cos \theta - \frac{22}{9}sk' \sin \theta)\eta_c^{-3} + O(\eta_c^{-4}), \end{aligned} \quad (23b)$$

$$\begin{aligned} \dot{\xi} = & -k' \sin \theta + (-2s + \frac{7}{6}sh'^{-1}k' \cos \theta)\eta_c^{-2} + (\frac{22}{3}h'^{-3}k' \cos \theta - \frac{3}{2}sk' \sin \theta)\eta_c^{-3} \\ & + [\frac{5}{2}sh'^2 - \frac{2}{2}sk'^2 + s(-\frac{59}{18}h'k' + \frac{14}{9}h'^{-5}k' + \frac{92}{3}h'^{-1}k'^3) \cos \theta \\ & + \frac{42}{12}h'^{-2}k' \sin \theta - \frac{5}{2}sk'^2 \cos 2\theta]\eta_c^{-4} + O(\eta_c^{-5}), \end{aligned} \quad (23c)$$

$$\begin{aligned} \dot{\eta} = & -\frac{3}{2}h' - 2k' \cos \theta + 2sh'^{-1}\eta_c^{-1} + (\frac{4}{3}h'^{-3} - \frac{7}{3}sh'^{-1}k' \sin \theta)\eta_c^{-2} \\ & + (-11sh' + \frac{16}{9}sh'^{-5} + \frac{7}{2}sh'^{-1}k'^2 - \frac{15}{2}sk' \cos \theta - \frac{56}{9}h'^{-3}k' \sin \theta)\eta_c^{-3} \\ & + [\frac{32}{3}h'^{-1} + \frac{80}{27}h'^{-7} + \frac{7}{3}h'^{-3}k'^2 + \frac{49}{36}h'^{-2}k' \cos \theta \\ & + s(\frac{353}{8}h'k' - \frac{28}{9}h'^{-5}k' - \frac{92}{18}h'^{-1}k'^3) \sin \theta + \frac{47}{8}sk'^2 \sin 2\theta]\eta_c^{-4} + O(\eta_c^{-5}) \end{aligned} \quad (23d)$$

with

$$\theta = t - \varphi'. \quad (24)$$

The relation between  $\eta_c$  and  $t$  is analogous to (17d)

$$\begin{aligned} t - \tau' = & -\frac{2}{3}h'^{-1}\eta_c - \frac{8}{3}sh'^{-3} \ln s\eta_c + \frac{16}{9}h'^{-5}\eta_c^{-1} + s(-\frac{22}{9}h'^{-1} + \frac{160}{81}h'^{-7})\eta_c^{-2} \\ & + (-\frac{224}{81}h'^{-3} + \frac{2240}{27}h'^{-9})\eta_c^{-3} + s(\frac{135}{4}h' - \frac{136}{27}h'^{-5} + \frac{448}{81}h'^{-11})\eta_c^{-4}. \end{aligned} \quad (25)$$

To obtain the parameters of the final motion, we must substitute the values obtained at the end of the numerical integration in the left sides of (23), and then solve these equations for  $h'$ ,  $k'$ ,  $\eta_c$ ,  $\theta$ . This is most conveniently done by an iteration technique. (23) is rewritten as

$$\begin{aligned} \xi = & h' + k' \cos \theta + f_1(h', k', \eta_c, \theta), \\ \eta = & \eta_c + f_2(h', k', \eta_c, \theta), \\ \dot{\xi} = & -k' \sin \theta + f_3(h', k', \eta_c, \theta), \\ \dot{\eta} = & -\frac{3}{2}h' - 2k' \cos \theta + f_4(h', k', \eta_c, \theta). \end{aligned} \quad (26)$$

The  $f_i$  represent small corrections of order  $\eta_c^{-1}$ . We invert (26) into

$$\begin{aligned} h' = & 4(\xi - f_1) + 2(\dot{\eta} - f_4), \\ \eta_c = & \eta - f_2, \\ k' \cos \theta = & 3(f_1 - \xi) + 2(f_4 - \dot{\eta}), \\ k' \sin \theta = & f_3 - \dot{\xi}. \end{aligned} \quad (27)$$

These equations are solved iteratively: starting with  $f_1 = f_2 = f_3 = f_4 = 0$ , we compute the left sides of (27); these values are used to recompute the  $f_i$ , which are defined by (23) and (26); the left sides are recomputed, and so on. The iteration converges quickly because of the smallness of the  $f_i$ .

Finally, if desired, the values of  $\tau'$  and  $\varphi'$  can be obtained from (25) and (24), with  $t_1$  substituted for  $t$ .

#### 2.4. Numerical Integration

The two satellites are considered here as point masses, and therefore can approach arbitrarily close to each other; for particular values of the impact parameter, they can even have a collision. To ensure a smooth and accurate numerical integration in such circumstances, we shift to regularized variables  $\hat{\xi}$ ,  $\hat{\eta}$ ,  $\hat{t}$ , whenever the distance  $\rho$  becomes less than a critical value  $\rho_c$ . The regularized variables are related to  $\xi$ ,  $\eta$ ,  $t$  by Levi-Civita's transformation (Szebehely, 1967):

$$\begin{aligned}\xi + i\eta &= (\hat{\xi} + i\hat{\eta})^2, \\ \frac{dt}{d\hat{t}} &= 4(\hat{\xi}^2 + \hat{\eta}^2).\end{aligned}\quad (28)$$

If we replace the cartesian coordinates  $\xi$ ,  $\eta$  by polar coordinates  $\rho$ ,  $\psi$ , then (28a) takes the simple form  $\rho = \hat{\rho}^2$ ,  $\psi = 2\hat{\psi}$ . Thus, regularization halves the polar angle  $\psi$ , and the hairpin turn made by  $M_3$  around  $M_2$  in a close approach is unfolded into a nearly straight motion. Simultaneously, the transformation (28b) on the time has the effect that the velocity, instead of reaching large values, remains nearly constant during a close approach.

At first the whole integration was made in regularized coordinates. Experience showed, however, that these coordinates are ill-adapted for large  $\rho$ ; the differential equations contain then large terms which nearly cancel each other, so that accuracy deteriorates. Therefore we revert to the normal coordinates  $\xi$ ,  $\eta$  when  $\rho$  becomes larger than  $\rho_c$ . The choice of  $\rho_c$  is not critical; a value  $\rho_c = 5$  was found to give good results.

A sixth-order predictor-corrector algorithm was used for the numerical integration, with automatic change of time step so that the variation of  $\Gamma$  in one time step is never more than a specified value. This was generally fixed at  $10^{-10}$ . The overall accuracy of the integration, according to various tests, is then of the order of  $10^{-9}$ .

#### 2.5. Computation of Minimal Distance

It is of interest to compute the minimal distance of approach of the two satellites. Therefore the value of  $\rho$  is monitored as the computation proceeds. A local minimum of  $\rho$  is detected from the fact that  $\rho$  at an integration point is smaller than at the preceding and following points. The true minimum is then computed by passing a straight line through the last two integration points and computing the distance from the origin to that line. This is done in regularized coordinates, so that the measured distance is actually the square root of  $\rho$ . This simple scheme gives quite accurate results, thanks to the fact that at the origin  $\hat{\xi} = \hat{\eta} = 0$ , there is

$$\begin{aligned}\frac{d^2\hat{\xi}}{d\hat{t}^2} &= 0, & \frac{d^2\hat{\eta}}{d\hat{t}^2} &= 0, \\ \frac{d^3\hat{\xi}}{d\hat{t}^3} &= -4\Gamma \frac{d\hat{\xi}}{d\hat{t}}, & \frac{d^3\hat{\eta}}{d\hat{t}^3} &= -4\Gamma \frac{d\hat{\eta}}{d\hat{t}},\end{aligned}\quad (29)$$

as is easily deduced from (8) and (28). Thus, the second derivative of the motion vanishes at the origin and the third derivative is parallel to the motion. The orbits are therefore quite straight in the vicinity of the origin. This is indeed apparent when the orbits are plotted in regularized coordinates.

### 3. RESULTS

#### 3.1. General Description

The one-parameter family of orbits obtained by varying  $h$  (family SE) was found to be of amazing complexity; in fact it seems to possess the inexhaustible richness of detail which is characteristic of nonintegrable problems in general. We begin with a loose description of the whole family; later we shall come back to interesting details.

Figures 1a to e, taken from a collection of several hundred pictures, represent the relative motion  $(\xi, \eta)$  of the two satellites. For their description, it will be convenient to think of the special case  $m_2 \gg m_3$ , and to identify the origin of the  $(\xi, \eta)$  system with the satellite  $M_2$ ; the curves represent then

simply the motion of satellite  $M_3$ . It should be borne in mind, however, that the results apply equally well for any mass ratio  $m_3/m_2$ .

Loosely speaking, three successive phases can be distinguished in a typical orbit: (i) *approach* of the two satellites; (ii) *interplay*, or *temporary capture*: the two satellites remain close to each other (their distance is of order 1 in Hill's coordinates) and they perform complex relative motions; (iii) *departure*: the two satellites move away from each other. Permanent capture was never observed: in all computed orbits, sooner or later the two satellites separated. This is in agreement with a general result by Marchal (1977) which can be applied to the present problem and which shows that *no permanent capture is possible, except for a set of initial conditions of measure zero*.

The departure is asymptotically described by (20), and two cases can be distinguished: (i) if  $h' > 0$ , then  $\eta \rightarrow -\infty$ , while  $\xi$  remains finite and oscillates around a positive mean value; this will be called *downward departure*; (ii) if  $h' < 0$ , then  $\eta \rightarrow +\infty$ , and  $\xi$  oscillates around a negative mean value; this will be called *upward departure*. When  $h$  varies, the orbit alternates from one kind of departure to the other, as will be seen.

We start with large values of  $h$ . The orbit of  $M_3$  is then only slightly perturbed. There is no interplay phase to speak of. Figure 1 shows an example for  $h = 2.4$ . The limit  $h \rightarrow \infty$  will be studied below in more detail (Section 3.4).

As  $h$  diminishes, the perturbation increases (Fig. 1,  $h = 1.9$ ) and a loop appears ( $h = 1.75$ ). The shape of the orbit begins to change rapidly with  $h$ . Between  $h = 1.7188$  and  $h = 1.7164$  approximately, the orbit undergoes a series of complex changes of shape. Typical examples are shown in Fig. 1. There is no obvious continuity along the family any more. In fact, it seems impossible to describe exhaustively the evolution of the family in this interval: as the resolu-

tion in  $h$  is increased, more and more changes of shape are revealed, apparently ad infinitum. We shall refer to this interval as the *first transition zone*; corresponding orbits in Fig. 1 are labeled zone I. Transition zones will be considered below in more detail (Section 3.6). The figure for  $h = 1.7187$  exhibits the first instance of an upward departure.

From  $h = 1.7164$  to  $h = 1.6664$  approximately, things quiet down and the evolution of the family can again be followed: the shape of the orbit changes continuously and comparatively slowly with  $h$ . Departure is upward. For the particular value  $h = 1.672987$ , we observe an orbit which is symmetrical with respect to the  $\eta$  axis. A number of such orbits have been found. This is not surprising: consider the value of  $\eta$  at a crossing with the  $\xi = 0$  axis. This value varies continuously with  $h$ . Whenever it becomes equal to zero, a symmetric orbit results, as is easily seen from the symmetries of the equations of motion (8).

Then a new interval of violent changes begins, between  $h = 1.6664$  and  $h = 1.6497$ . This will be called the second transition zone (zone II in Fig. 1). Typical shapes are illustrated in Fig. 1. The figure for  $h = 1.6646$  shows a case where the temporary capture is of unusually long duration.

A new quiet interval follows, from  $h = 1.6497$  to  $h = 1.5931$ . Departure is again upwards. There is an orbit symmetric with respect to the  $\eta$  axis at  $h = 1.631825$ . The orbit describes two loops around  $M_2$  until  $h = 1.620191$  and only one loop afterward; this particular value of  $h$  corresponds to a collision orbit, i.e., an orbit in which  $M_3$  coincides with  $M_2$  at a particular time. This kind of orbit exists only in the present mathematical idealization, where the satellites are considered as point masses; with real objects, having a finite size, a physical collision would take place before that time and the ensuing course of events would be entirely different (see Section 3.3). As is well known (see, for instance, Szebehely, 1967), a collision orbit is not a true singular-

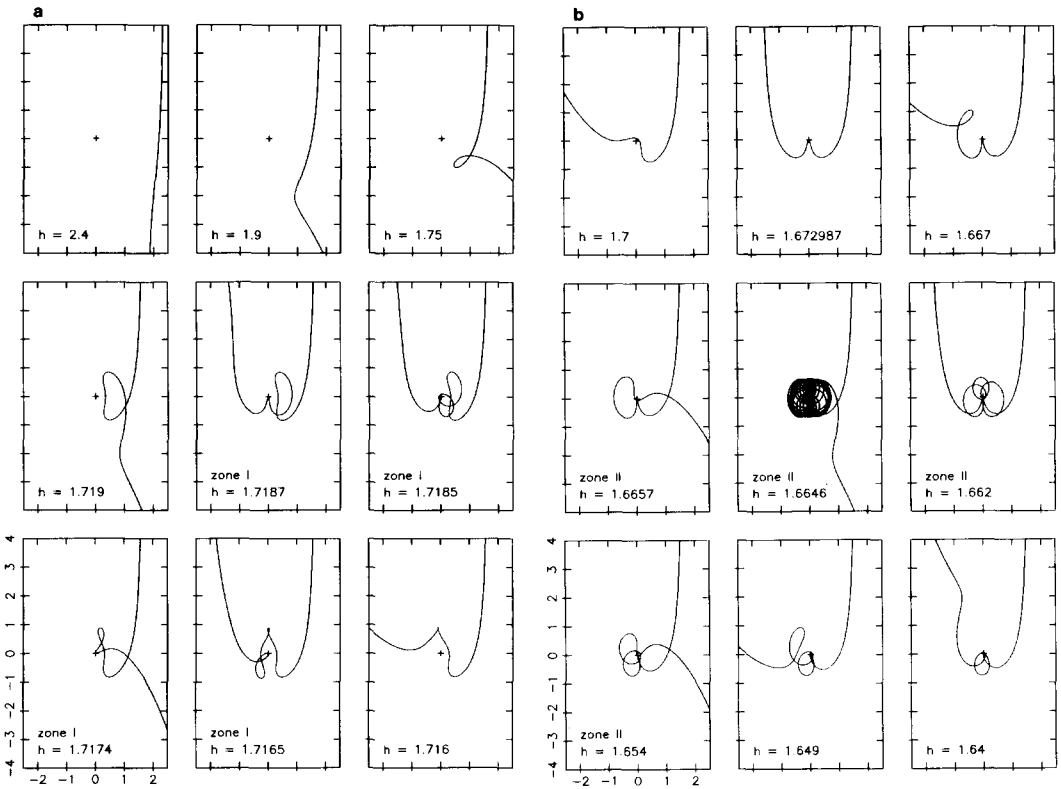


FIG. 1. (a) Beginning of family SE (satellite encounters). Each frame corresponds to one particular value of the reduced impact parameter  $h$ . The curve represents the relative motion of one satellite with respect to the other, in Hill's coordinates ( $\xi$  in abscissa,  $\eta$  in ordinate). The initial approach is downwards from  $\eta = +\infty$ , in the first quadrant. Orbits belonging to transition zones are labeled zone I, zone II, zone III, zone IV. (b) Continuation of family SE.

ity: a family of orbits can be smoothly continued through a collision orbit. In regularized coordinates, everything remains finite, and the numerical integration can proceed right through the collision orbit without any problem.

The third transition zone is contained in the interval from  $h = 1.5931$  to  $h = 1.5918$ . Typical orbits are shown in Fig. 1.

There follows a much longer period of quiet, from about  $h = 1.5918$  to  $h = 1.3486$ . The orbit has a simple shape. Departure is downward. At  $h = 1.446862$ , we find a collision orbit. At  $h = 1.514780$  and again at  $h = 1.375290$ , the orbit is symmetric with respect to the  $\xi$  axis. Again a number of such orbits have been found, and again this can be explained by the symmetries of the equa-

tions (8): a symmetric orbit is obtained whenever  $\dot{\xi}$  vanishes at a crossing with the  $\xi$  axis.

The fourth and last transition zone lies in the interval from  $h = 1.3486$  to  $h = 1.3361$ ; some orbits are shown in Fig. 1.

From  $h = 1.3361$  to  $h = 0$ , the evolution of the orbit is smooth. On a given orbit,  $\eta$  decreases to a minimal value along the orbit, and then increases again to infinity. In the limit of small  $h$ , we obtain "horseshoe orbits" (see Section 3.5). The interplay phase vanishes again. The minimum of  $\eta$  increases rapidly and tends to  $+\infty$  for  $h \rightarrow 0$ .

It should be noted that there is nothing absolute about the limits of the transition zones, as described above, nor even about

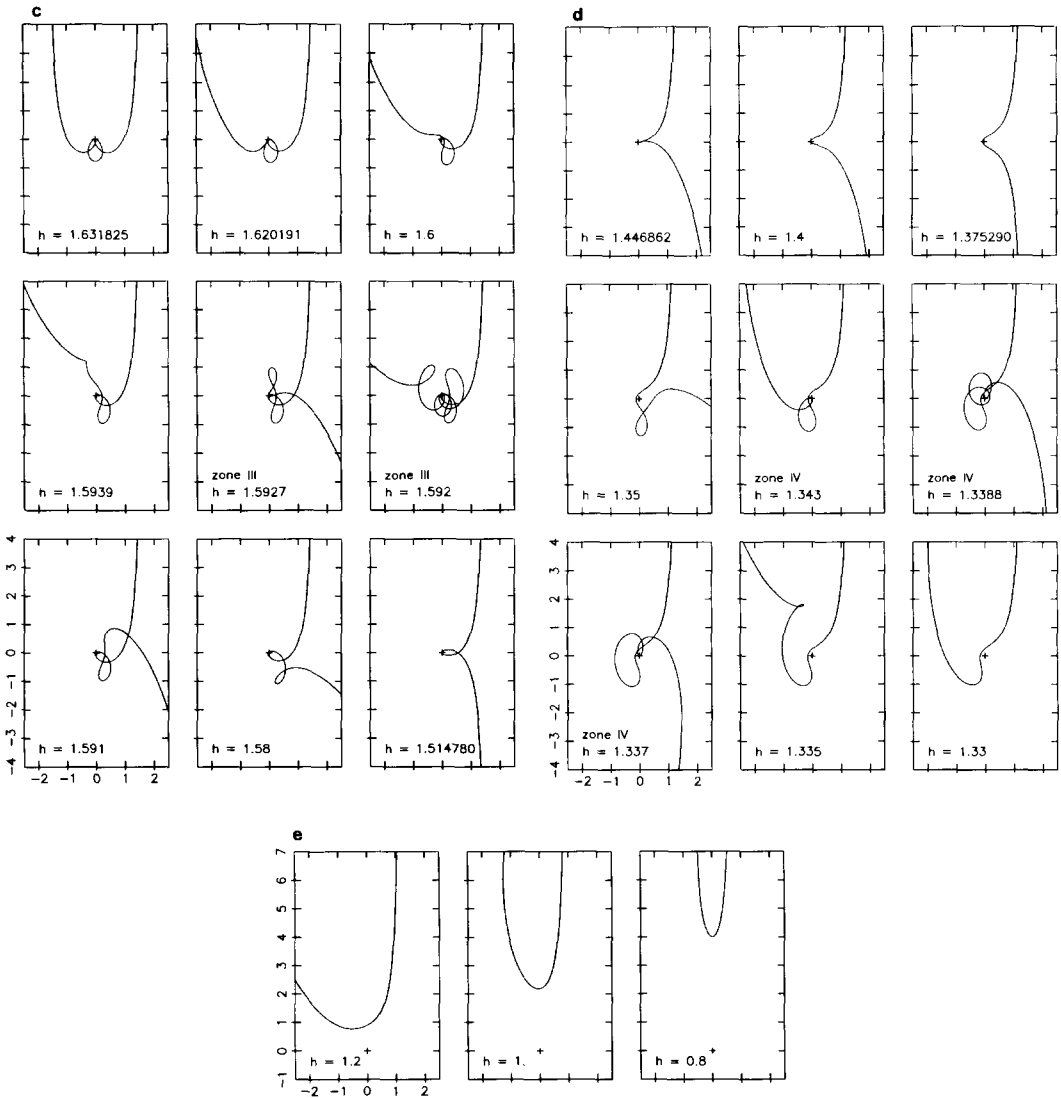


FIG. 1—Continued. (c) Continuation of family SE. (d) Continuation of family SE. (e) Continuation of family SE. Note that the frame is not the same as in previous figures.

their number. The description was given at a somewhat arbitrarily chosen level of detail. When descending to a finer level, one finds that each of the above transition zones is resolved into several thinner transition regions, separated by quiet regions. For instance, inside the fourth transition zone, one can isolate two smaller transition regions, contained in the intervals (1.3486, 1.3482) and (1.3397, 1.3361), outside of

which the evolution is smooth. This phenomenon of finer and finer structure apparently goes on indefinitely, suggesting that the true transitions have the structure of a Cantor set (see Section 3.6).

### 3.2. Final Effect of the Encounter

The net effect of the encounter is essentially characterized by the changes in the reduced impact parameter  $h$  and the re-

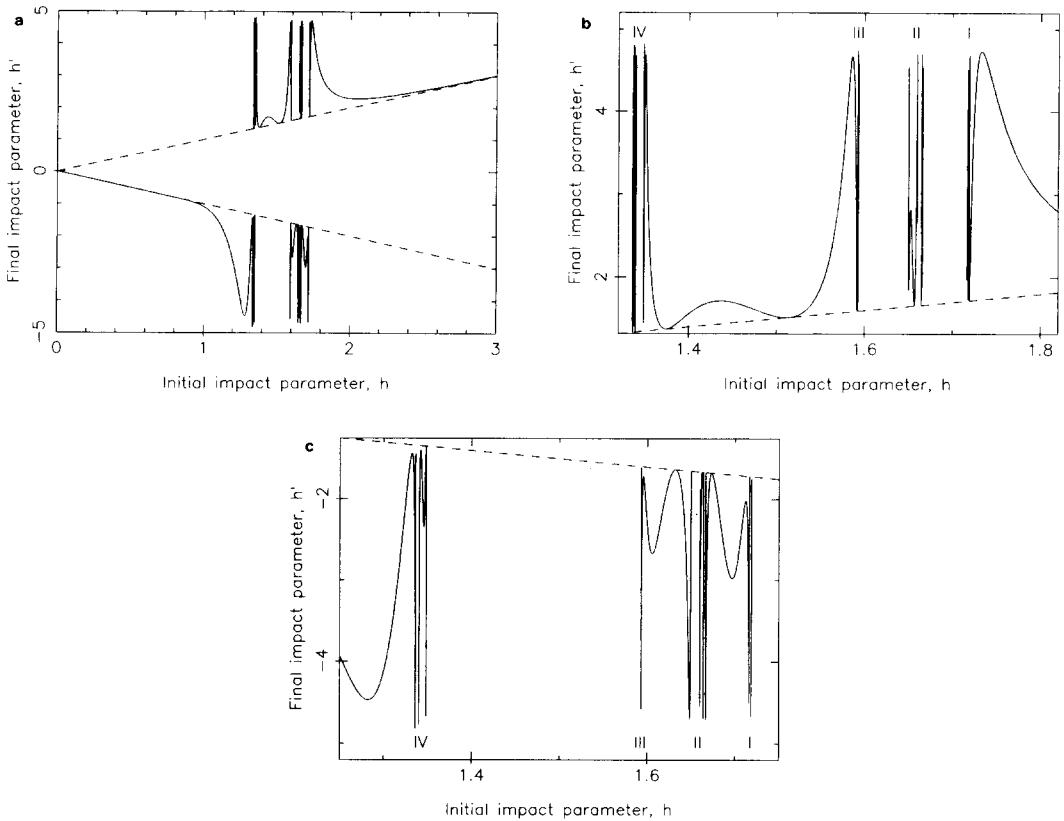


FIG. 2. (a) Final impact parameter  $h'$  as a function of the initial impact parameter  $h$ . The region between the two dashed lines is forbidden. (b) Enlargement of part of Fig. 2a. I, II, III, IV: transition zones. (c) Enlargement of part of Fig. 2a. I, II, III, IV: transition zones.

duced eccentricity  $k$ . These changes are not independent: from (9) and (12) we have for  $t \rightarrow -\infty$ , i.e., before the encounter

$$\Gamma = \frac{3}{4}h^2, \tag{30}$$

while from (9) and (20) we have for  $t \rightarrow +\infty$ , i.e., after the encounter

$$\Gamma = \frac{3}{4}h'^2 - k'^2. \tag{31}$$

Therefore

$$\Delta(h^2) = h'^2 - h^2 = \frac{3}{4}k'^2. \tag{32}$$

Thus  $|h'| \geq |h|$ : the radial separation of the two satellites can only increase under the effect of the encounter. This asymmetrical behaviour is due to our assumption that the orbits are initially circular; if arbitrary initial orbits were allowed, (30) would have to

be replaced by the more general relation

$$\Gamma = \frac{3}{4}h^2 - k^2 \tag{33}$$

where  $k$  is the initial reduced eccentricity, and the radial separation could decrease as well as increase (Petit, 1985).

Figure 2a represents  $h'$  as a function of  $h$ . The dashed lines correspond to  $h' = h$  and  $h' = -h$ ; the region between these lines is empty, as dictated by (32). For large  $h$ ,  $h' \approx h$  (see Section 3.4); for small  $h$ ,  $h' \approx -h$  (see Section 3.5). The upper part of the figure corresponds to downward departure; it is shown enlarged in Fig. 2b. The lower part of the figure corresponds to upward departure, and is shown enlarged in Fig. 2c. The transition zones described in Section 3.1 correspond to regions of violent change of

$h'$  in Fig. 2. The curve touches several times the lines  $h' = \pm h$ . These particular points correspond to symmetric orbits, for which there is  $k' = k = 0$ , and therefore  $h'^2 = h^2$ .

Figure 3 shows the final eccentricity  $k'$  as a function of the initial impact parameter  $h$ . This figure is closely related to Fig. 2 because of the relation (32).  $k'$  tends to zero for both  $h \rightarrow 0$  and  $h \rightarrow \infty$ . An interesting observation is that  $k'$  seems to be bounded from above: it exhibits several maxima with values nearly equal and slightly below 4.

Equation (32) represents a transfer of energy: an increase of the radial separation of the satellites corresponds to a decrease of the potential energy of the system, as is easily shown (Brahic, 1977), while an increase of  $k$  represents an increase of the kinetic energy. This process is of fundamental importance for the long-term evolution of planetary rings (Brahic, 1977). It can be shown (Petit, 1985) that the rate of transfer of energy, in a ring system composed of many particles of equal mass, is proportional to the integral

$$I = \int_0^\infty h \Delta(h^2) dh. \tag{34}$$

This integral can be evaluated from the present results, and we quote its value for future use:

$$I = 7.77. \tag{35}$$

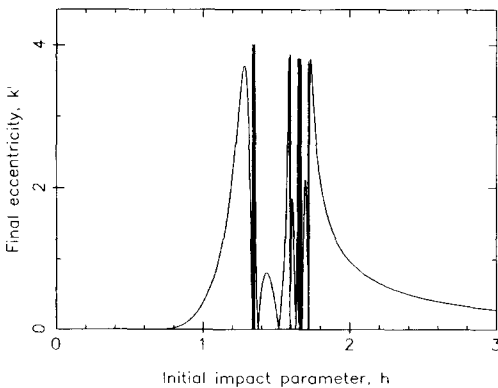


FIG. 3. Final eccentricity  $k'$  as a function of the initial impact parameter  $h$ .

This value is not very accurately determined, because of the wild fluctuations of  $h$  in the transition regions.

### 3.3. Minimal Distance of Approach

In the present paper, the two satellites have been considered as points without dimensions. They can therefore approach each other at an arbitrarily small distance; this distance even becomes zero in collision orbits. In an astronomical application, the actual size of the satellites should be taken into account. If we assume for simplicity that the satellites are spherical, with radii  $r_2$  and  $r_3$ , then any one of the orbits presented here will be physically meaningful only if the distance between the satellites never becomes less than  $r_2 + r_3$ . In Hill's coordinates, the radii of the satellites are  $\rho_2$  and  $\rho_3$  defined by

$$r_2 = a_0 \mu^{1/3} \rho_2, \quad r_3 = a_0 \mu^{1/3} \rho_3, \tag{36}$$

and the condition for the existence of the orbit is

$$\rho_{\min} > \rho_2 + \rho_3, \tag{37}$$

where  $\rho_{\min}$  is the minimal distance of approach of the two satellites. The condition (37) excludes all collision orbits, as well as a finite interval in  $h$  around each of them (and possibly other intervals).

If condition (37) is violated, the two satellites come into contact at some time  $t_c$ . The part of the computed orbit corresponding to  $t < t_c$  is still valid; but for  $t > t_c$  the course of events will be entirely different. Depending on physical conditions, the two satellites might accrete, or explode into fragments, or bounce inelastically; these developments will not be considered in the present paper. Petit and Hénon (1986; see also Petit, 1985) have made a detailed study of satellite interactions when both attraction and inelastic rebounds are taken into account.

The quantity  $\rho_{\min}$  is therefore of interest, and is computed for each orbit. Figure 4 represents  $\rho_{\min}$  as a function of  $h$ . The vertical scale is logarithmic, to better show

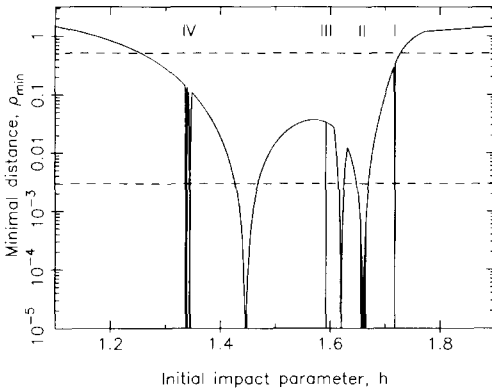


FIG. 4. Minimal distance of approach as a function of the initial impact parameter  $h$ . Lower dashed line: critical distance for collision of interplanetary particles with the Earth. Upper dashed line: critical distance for collision of two typical particles in Saturn's rings. I, II, III, IV: transition zones.

small values of  $\rho_{\min}$ . (A similar figure, showing less detail, has been published by Schofield (1981).) For large  $h$ ,  $\rho_{\min} \approx h$ ; for small  $h$ ,  $\rho_{\min} \approx 8/3h^2$  (see Section 3.5). The transition regions are again characterized by violent changes; however, the variation of  $\rho_{\min}$  seems to be generally smoother than that of  $h'$  or  $k'$ . Collision orbits correspond to  $\rho_{\min} = 0$ ; there are three conspicuous cases at  $h = 1.446862$ ,  $h = 1.620191$ , and  $h = 1.660405$ . Other collisions (in infinite number) take place in the transition regions. Discontinuities in the slope of the curve can be seen in several places; this corresponds to one local minimum of  $\rho_{\min}$  on the orbit displacing another as the global minimum.

As an example of the use of this figure, we consider the problem of the accretion of interplanetary particles by the Earth. Bodies  $M_1$ ,  $M_2$ ,  $M_3$  are the Sun, the Earth, and the particle, respectively. The problem is idealized by assuming that the orbits of the Earth and of the particle are circular. The radius of the particle can be neglected. Substituting numerical values into (36) and (37), we obtain

$$\rho_{\min} > 0.00295. \quad (38)$$

This critical value is represented by the

lower dashed line in Fig. 4. Values of  $h$  for which the curve lies below this line correspond to interplanetary particles which collide with the Earth. This happens in three large intervals associated with the three above-mentioned collision orbits, and also in a number of smaller intervals associated with transition regions. These intervals correspond to the bands found by Dole (1962, Table 2).

As another example, we consider the interaction of two particles in Saturn's rings. Taking  $a_0 = 10^5$  km and assuming a particle density of  $1 \text{ g cm}^{-3}$ , we obtain

$$\rho > 0.514 \frac{r_2 + r_3}{(r_2^3 + r_3^3)^{1/3}}. \quad (39)$$

The right side depends only on the relative size of the particles. For two identical particles, we obtain

$$\rho > 0.816, \quad (40)$$

while if one particle is much larger than the other, we have

$$\rho > 0.514. \quad (41)$$

This last limit is shown as the upper dashed line in Fig. 4. Clearly collisions play a dominant role in this case.

### 3.4. Large Impact Parameter

When the impact parameter  $h$  is sufficiently large, the encounter produces only small deflections of the orbits (see Fig. 1 for  $h = 2.4$ ), and a perturbation theory can be applied. This theory has been given by Goldreich and Tremaine (1980), for the case where one of the satellites has a negligible mass compared to the other. The result is easily generalized to the case of an arbitrary mass ratio (see Paper I); in Hill's coordinates, one obtains

$$\begin{aligned} h' &= h + \frac{1}{243} [2K_0(\frac{2}{3}) + K_1(\frac{2}{3})]^2 h^{-5} \\ &= h + 3.34379 h^{-5} \end{aligned} \quad (42)$$

where  $K_0$  and  $K_1$  are modified Bessel functions.

Table I compares the values of  $h' - h$  obtained by numerical integration with the

TABLE I  
COMPARISON OF NUMERICAL AND THEORETICAL RESULTS FOR LARGE  $h$

$h$	$h' - h$	$3.34379h^{-5}$
3	0.0172311	0.0137605
4	0.00357307	0.00326542
5	0.00111960	0.00107001
6	0.000441348	0.000430014
7	0.000202225	0.000198952
8	0.000103163	0.000102044
9	0.0000570624	0.0000566274
10	0.0000336248	0.0000334379

values predicted by (42). It can be seen that (42) correctly describes the asymptotic behavior of  $h'$  for  $h \rightarrow \infty$ . In fact it is a good representation even for moderately high values of  $h$ : at  $h = 10$ , the relative error is already less than 1%.

Moreover, the difference between the computed and theoretical values appears to behave asymptotically as  $18.7h^{-8}$  approximately, suggesting that (42) is the beginning of a series of the form

$$\frac{h'}{h} = 1 + 3.34379h^{-6} + 18.7h^{-9} + \dots \tag{43}$$

An extension of the theory might be able to account for this.

3.5. Small Impact Parameter

When the impact parameter is small, the orbit assumes the well-known ‘‘horseshoe’’ shape (see, for instance, the last frame in Fig. 1). It is almost exactly symmetrical with respect to the  $\eta$  axis. A first-order perturbation theory (see Paper I) gives the following equation for the orbit:

$$\eta(h^2 - \xi^2) = \frac{8}{3}. \tag{44}$$

This is indeed symmetrical. Equation (44) shows also that the minimal distance between the satellites is reached at the  $\eta$ -axis crossing, and is

$$\rho_{\min} = \frac{8}{3h^2}. \tag{45}$$

In fact a much stronger result can be demonstrated: it can be shown that an adiabatic invariant exists for  $h \rightarrow 0$  (Paper I). The conservation of this adiabatic invariant implies the symmetry of the orbit, and in particular:  $h' = -h$  and  $k' = 0$ . A theoretical computation (see Paper I) gives the following asymptotic expression of the final eccentricity  $k'$  for  $h \rightarrow 0$ :

$$k' = 2^{2/3} 3^{-3/2} 5 \Gamma(\frac{2}{3}) \exp\left(-\frac{8\pi}{9h^3}\right). \tag{46}$$

Thus,  $k'$  decreases extremely rapidly for  $h \rightarrow 0$ , faster than any power of  $h$ . Figure 5 shows that (46) agrees reasonably well with the numerical results, although the convergence to the asymptotic form seems to be rather slow.

3.6. Transition Zones

Figure 1 shows that, as  $h$  is varied, the departure of  $M_3$  sometimes changes suddenly from downwards to upward, or conversely. This will be called a *transition*. We will now analyze transitions in some detail and explain their origin.

First we shall refine the definition of a transition just given. We use again a system  $\rho, \psi$  of polar coordinates in the  $\xi, \eta$  plane. Let  $\Delta\psi$  be the total variation of  $\psi$ , from  $t = -\infty$  to  $t = +\infty$ . Both ends of the orbit correspond to  $\eta \rightarrow \pm\infty$ , with  $\xi$  finite, as shown

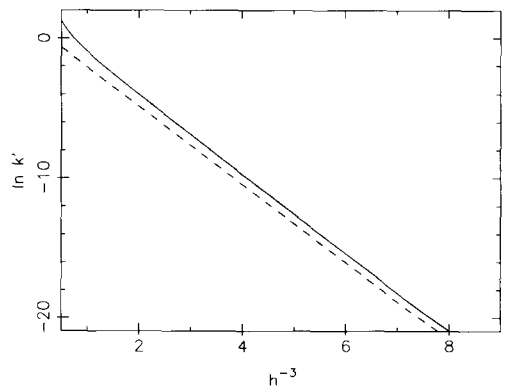


FIG. 5. Full line: final eccentricity for small values of the impact parameter. Dashed line: asymptotic formula (46).

by equations (12) and (20); therefore  $\Delta\psi$  is a multiple of  $\pi$ . In general, a small change in  $h$  does not change the value of  $\Delta\psi$ . Across some particular values of  $h$ , however,  $\Delta\psi$  changes discontinuously by a multiple of  $\pi$ . A first obvious case is that of collision orbits. A simple analysis shows (see Petit (1985) for detailed illustrations) that the change of  $\Delta\psi$  across a collision orbit is  $\pm 4\pi$ . We want to exclude collision orbits from our considerations, since they are not true singularities (as already mentioned). This suggests that we define the *index* of an orbit as

$$j = \frac{\Delta\psi}{\pi} \pmod{4}. \tag{47}$$

$j$  can take the values 0, 1, 2, 3. This index is invariant in any interval where the orbit changes continuously with  $h$ , including passages through collision orbits. Conversely, a change in the index means that the family SE has suffered a discontinuity of some kind. So we redefine a *transition* as a change in  $j$ . Note that with this new definition we catch more transitions than with the earlier one, since we have now four classes of orbits ( $j = 0, 1, 2, 3$ ) instead of two (departure upward or downward). The old definition was equivalent to distinguishing only between  $j$  odd or even.

In regularized coordinates, the index has a simple meaning: the regularized polar angle is  $\hat{\psi} = \psi/2$ , and therefore the values 0, 1, 2, 3 of the index correspond to a departure in the first, second, third, and fourth quadrants, respectively.

Table II gives observed values of the index  $j$ , at a resolution of  $10^{-4}$  in  $h$ . Each line refers either to an interval in which family SE appears to be continuous (and therefore has a constant  $j$ ), or to a single value of  $h$ . The existence of many transitions is apparent. Note that this is not an exhaustive tabulation of the  $j$  values: in every interval of width  $10^{-4}$  separating one line from the next, an arbitrary number of transitions can take place.

The presence of these transitions is puz-

TABLE II  
INDEX  $j$  AS A FUNCTION OF THE IMPACT  
PARAMETER  $h$

$h$	$j$	$h$	$j$
$\infty$ to 1.7188	3	1.6497 to 1.5931	2
1.7187	0	1.5930 to 1.5922	3
1.7186 to 1.7184	2	1.5921 to 1.5920	0
1.7183 to 1.7166	1	1.5919	2
1.7165	2	1.5918 to 1.3486	1
1.7164 to 1.6664	0	1.3485 to 1.3484	3
1.6663 to 1.6647	1	1.3483	0
1.6646	2	1.3482 to 1.3397	2
1.6645	0	1.3396	0
1.6644	2	1.3395 to 1.3381	3
1.6643	1	1.3380 to 1.3377	0
1.6642	1	1.3376 to 1.3375	1
1.6641 to 1.6600	0	1.3374	2
1.6599 to 1.6501	3	1.3373	2
1.6500 to 1.6499	0	1.3372 to 1.3362	1
1.6498	3	1.3361 to 0	0

zling at first view. The differential equations (8) contain no true singularities, since the apparent singularity at the origin can be removed by regularization. Therefore the position of body  $M_3$  after a given time should be a continuous function of its initial position and velocity. How then is it possible for the final motion to jump from upwards to downwards when  $h$  changes continuously?

This paradox provides in fact the clue: it indicates that to achieve a transition, we must pass through an orbit for which the duration of the “temporary capture” is infinite. One way to achieve this is that *the orbit tends asymptotically toward a periodic orbit*.

This is confirmed by numerical results. Figure 6 represents, as an example, the orbit for

$$h = 1.718779940 \tag{48}$$

which is the first transition encountered when coming from high values of  $h$ . The orbit is seen to tend toward a kidney-shaped periodic orbit. This limiting orbit is easily identified: it belongs to the one-parameter family  $a$  of periodic orbits, emanat-

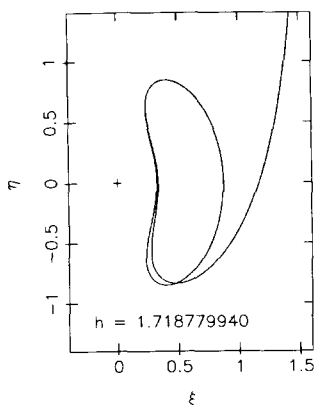


FIG. 6. An orbit of family SE which is asymptotic to an unstable periodic orbit.

ing from the Lagrangian point  $L_2$  (Hénon, 1969, Fig. 2). The value of the Jacobi constant is given by (30)

$$\Gamma = 2.215653362. \tag{49}$$

This value identifies the particular orbit of family  $a$  which is involved here.

It will be helpful to introduce at this point a *surface of section*, defined for instance by  $\eta = 0, \dot{\eta} > 0$  (Hénon, 1970): for each crossing of an orbit with the  $\xi$  axis in the positive direction ( $\eta$  increasing), we plot a point with coordinates  $\xi, \dot{\xi}$  (Fig. 7). An orbit is then represented by a sequence of points. For a given value of  $\Gamma$ , a point in the surface of section defines completely the corresponding orbit:  $\xi, \dot{\xi}, \eta$  are immediately known and  $\dot{\eta}$  can be computed from (9). In particular, the next intersection point can be found. This defines a mapping of the surface of section onto itself, known as a *Poincaré map*.

Note that an encounter-type orbit of the kind considered in the present paper corresponds in general to a finite sequence of points in the surface of section; for instance the orbit for  $h = 1.7187$ , Fig. 1a, corresponds to a sequence of three points. Therefore a point of the surface of section does not always have an image in the Poincaré map. Similarly, it does not always have an antecedent. The sequence can even

be empty, as for instance for  $h = 2.4$ , Fig. 1a.

We consider in particular the Poincaré map corresponding to the value (49) of  $\Gamma$ . The periodic orbit corresponds to a fixed point  $P$  of this map. This periodic orbit must be unstable since it admits an asymptotic orbit. Indeed its stability index is of the order of 320 (Hénon, 1969, Table 2), corresponding to two real eigenvalues  $\lambda_1 \approx 1/640$  and  $\lambda_2 \approx 640$ . The eigenvalue smaller than 1 in modulus ( $\lambda_1$ ) is associated with a one-parameter family of *incoming orbits* tending towards the periodic orbit. The orbit of Fig. 6 is a member of this family. (A picture of the whole family can be obtained by applying a symmetry with respect to the horizontal axis to Figs. 8a and b.) In the surface of section, an incoming orbit is represented by an infinite sequence of points  $Y_0, Y_1, Y_2, \dots$ , which lie on a curve  $W_s$  known as the *stable invariant manifold* of  $P$ , and which converge exponentially on  $P$  (Fig. 7).

The eigenvalue larger than 1 in modulus ( $\lambda_2$ ) is associated with a one-parameter family of *outgoing orbits*, which tend toward the periodic orbit for  $t \rightarrow -\infty$ . For  $t$  increasing, these orbits emerge from the periodic orbit and go away at an exponential rate. The family of outgoing orbits is shown in

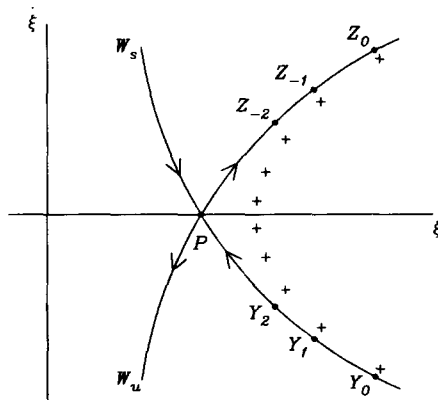


FIG. 7. Sketch of the surface of section. The value of  $\lambda_1$  has been artificially increased to show the structure more clearly.

Figs. 8a and b. In the surface of section, an outgoing orbit corresponds to a sequence of points . . . ,  $Z_{-2}$ ,  $Z_{-1}$ ,  $Z_0$ , infinite toward the past, which lie on the *unstable invariant manifold*  $W_u$  of  $P$  and which diverge exponentially from  $P$  (Fig. 7).

Consider now an orbit of family SE with a value of  $h$  slightly larger than (48). Corresponding points in the surface of section will be slightly displaced. Also,  $\Gamma$  will be slightly different from the value (49), so that there will be a small displacement of the periodic orbit, of the fixed point  $P$ , and of the invariant manifolds  $W_s$  and  $W_u$ . As a result, the points in the surface of section will lie slightly besides  $W_s$ ; examination shows that they lie to the right of  $W_s$  (crosses in Fig. 7). They will remain close to it until they reach the vicinity of  $P$ ; then they go away, approaching closely  $W_u$ . Now a crucial fact is that  $\lambda_2$  is positive; therefore the points go away along one branch only of  $W_u$ . For  $h$  larger than (48), this is the upper right branch of  $W_u$ .

Consider next a value of  $h$  slightly smaller than (48). Then the approaching points lie slightly to the left of  $W_s$ , and after reaching the vicinity of  $P$  they go away along the lower left branch of  $W_u$ . Thus,

when  $h$  crosses the critical value (48), the points suddenly jump from one branch of  $W_u$  to the other. The two branches lead the orbit into entirely different regions of phase space. This is essentially the explanation of how transitions arise.

We note again that only the asymptotic behaviour of the points for  $t \rightarrow +\infty$  is discontinuous at a transition; the position of any given point is a continuous function of  $h$ . As  $h$  approaches the critical value, the orbit spends more and more time in the vicinity of the periodic orbit; in the surface of section, the points accumulate near  $P$  before finally moving away.

We remark incidentally that the incoming orbit of Fig. 6 belongs to the set of measure zero of orbits undergoing permanent capture (see Section 3.1). Figure 6 seems to contradict our earlier assertion that permanent capture was never observed. Actually it does not. The computed orbit, represented on Fig. 6, differs very slightly from the exact asymptotic orbit because the value (48) can only be specified with finite accuracy and also because of numerical errors. As a consequence, after having made a finite number of loops in the close vicinity of the periodic orbit, it departs to infinity.

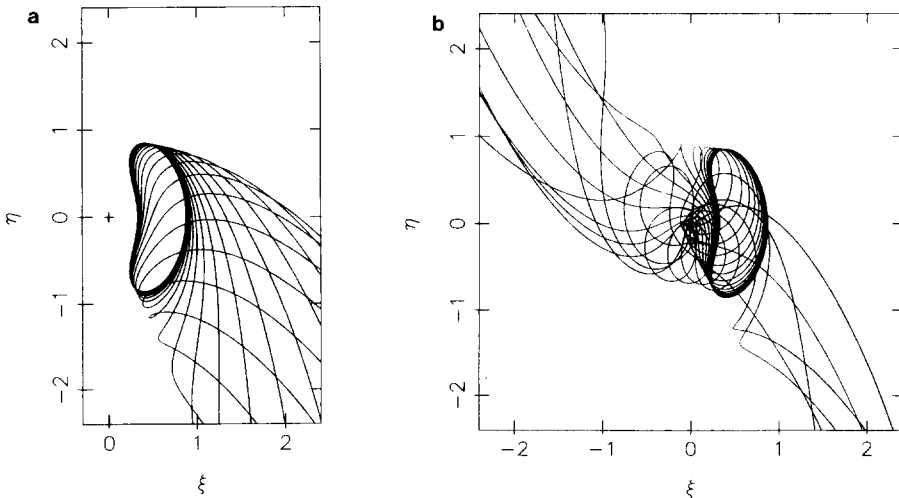


FIG. 8. (a) Outgoing orbits for  $h$  above the critical value (48). (b) Outgoing orbits for  $h$  below the critical value (48).

To obtain Fig. 6 it was necessary to interrupt the integration at an appropriate time (the fifth crossing of the  $\xi$  axis was chosen).

Figures 8a and b represent the outgoing orbits separately for each branch of  $W_u$ . In each case we have a cyclic family. Figure 8a corresponds to values of  $h$  larger than (48). The points move away from  $P$  along the upper right branch of  $W_u$  in Fig. 7. The family has a simple structure in this case, and all outgoing orbits depart in the downward direction. Figure 8b corresponds to values of  $h$  smaller than (48). The points move away along the lower left branch of  $W_u$ . It is apparent that the behaviour is completely different from that of Fig. 8a. It is also much more complicated. The orbits depart sometimes upward, sometimes downward.

This last fact indicates that the true situation is even more complex than the above description would suggest. Instead of departing immediately, the outgoing orbit may well encounter another unstable periodic orbit; this will again give rise to a transition, which might be called a *second-order transition* since now two unstable periodic orbits are involved. In this way, a hierarchical structure of transitions of higher and higher order is built. We remark also that as  $h$  approaches a critical value such as (48), essentially the same outgoing orbit is obtained for an infinite sequence of  $h$  values, forming a geometrical progression of ratio  $\lambda_1$  (see Petit (1985) for illustrations). This gives rise to a self-similar, Cantor-like structure for the set of the transitions. We shall not dwell further here on this subject, which we plan to explore in a future paper.

### 3.7. Comparison with Earlier Results

The present results are essentially in agreement with earlier computations. There are, however, minor quantitative differences, due to the fact that different approximations have been used. It is of interest to investigate these differences: this shows the effect of the approximations.

Giuli (1968a, Table I) gives values for the

boundaries of the major “bands” in which interplanetary particles hit the Earth. It will be convenient to use these values as a basis for the comparison. Three different cases have been considered by Giuli. In case 1, the Earth has its present mass; this corresponds to  $\mu^{1/3} = 0.01443$  in our notation. The numerical integration starts at 0.215 a.u., corresponding to  $\eta_0 = 14.9$  in our units. In case 2, the initial distance is increased to 0.5 a.u., corresponding to  $\eta_0 = 34.7$ . Case 3 corresponds to an “early-stage” Earth, with a mass smaller by a factor 1000 and with the initial distance still equal to 0.5 a.u.; this corresponds to  $\mu^{1/3} = 0.001443$  and  $\eta_0 = 347$ . The boundaries found by Giuli for the different cases are translated into Hill’s coordinates by the relation  $a = 1 + \mu^{1/3}h_G$  and are reproduced in Table III, column 2.

In the present paper, these bands correspond to the two major intervals of  $h$  for which  $\rho_{\min}$  becomes less than 0.00295, around the collision orbits at  $h = 1.446862$  and  $h = 1.660405$  (see Section 3.3 and Fig. 4). The boundaries  $h_p$  found by us are given in Table III, column 3. The value is the same in all three cases, since in Hill’s formalism the solution does not depend on the masses of the satellites, and since the orbit as computed in the present paper is not affected by the choice of the initial value  $\eta_0$ . Note also that in Hill’s case one obtains symmetrical values of  $h$  for “inner bands” ( $h < 0$ ) and “outer bands” ( $h > 0$ ).

$|h_G|$  is always smaller than  $|h_p|$ ; this is most pronounced in case 1. This is a consequence of the fact that in Giuli’s computations, the integration was started at a not very large distance,  $\eta_0 = 14.9$ , with the particle still on its circular orbit. In other words, the attraction of the Earth between  $\eta = \infty$  and  $\eta = 14.9$  was ignored. This produces an error of the order of  $\eta_0^{-1}$ , as shown by (17). A first-order correction can be applied to Giuli’s values, using the second term in (17):

$$h_{GC} = h_G + \frac{1}{3}h_p^{-1}\eta_0^{-1}. \quad (50)$$

TABLE III

COMPARISON WITH THE RESULTS OF GIULI (1968a)

Case	$h_G$	$h_P$	$h_{GC}$	$h_{PC}$
1	-1.6020	-1.6702	-1.6556	-1.6558
2	-1.6296	-1.6702	-1.6526	-1.6558
3	-1.6660	-1.6702	-1.6683	-1.6688
1	-1.5794	-1.6484	-1.6337	-1.6340
2	-1.6072	-1.6484	-1.6305	-1.6340
3	-1.6445	-1.6484	-1.6468	-1.6470
1	-1.3912	-1.4688	-1.4521	-1.4544
2	-1.4291	-1.4688	-1.4553	-1.4544
3	-1.4643	-1.4688	-1.4669	-1.4674
1	-1.3476	-1.4273	-1.4103	-1.4129
2	-1.3878	-1.4273	-1.4147	-1.4129
3	-1.4234	-1.4273	-1.4261	-1.4259
1	1.3702	1.4273	1.4329	1.4417
2	1.4418	1.4273	1.4387	1.4417
3	1.4262	1.4273	1.4289	1.4287
1	1.4150	1.4688	1.4759	1.4832
2	1.4537	1.4688	1.4799	1.4832
3	1.4671	1.4688	1.4697	1.4702
1	1.6097	1.6484	1.6640	1.6628
2	1.6381	1.6484	1.6614	1.6628
3	1.6480	1.6484	1.6503	1.6498
1	1.6330	1.6702	1.6866	1.6846
2	1.6605	1.6702	1.6835	1.6846
3	1.6695	1.6702	1.6718	1.6716

The corrected values are shown in column 4 of Table III. The agreement is now much better.

The remaining difference  $h_{GC} - h_P$  is always positive, and therefore corresponds to an asymmetrical effect:  $|h_{GC}| < |h_P|$  for inner orbits,  $|h_{GC}| > |h_P|$  for outer orbits. Also it is approximately ten times smaller in case 3 than in cases 1 and 2, and therefore proportional to  $\mu^{1/3}$ . This difference is most likely a consequence of the substitution of Hill's equations for the exact three-body equations in the present paper. This substitution introduces errors of the order of  $\mu^{1/3}$  (see Paper I), and as is easily seen, the

dominant error term is quadratic in  $\xi$  and  $\eta$  and therefore has a constant sign.

An empirical correction can be applied to our values:

$$h_{PC} = h_P + b\mu^{1/3} \tag{51}$$

where  $b$  is a constant, to be adjusted in an ad hoc fashion. It was found that  $b = 1$  gives satisfactory results. The corresponding values of  $h_{PC}$  are given in column 5 of Table III. The agreement between columns 4 and 5 is quite good in most cases.

A similar comparison can be carried out with the results of Dole (1962, Table 2), who gives values for seven inner bands. Exactly the same effects are found.

### 3.8. Noncircular Motions

A natural generalization of the present work would be to consider the case where the two satellites are initially on elliptical orbits. Unfortunately the number of essential parameters jumps then from one to three. The asymptotic form of the motion before the encounter is given by an expression identical to (20), with the primes suppressed. It depends on four arbitrary parameters  $h, k, \varphi, \tau$ . The parameter  $\tau$  can be eliminated by a change of the origin of time, but we are still left with three parameters: the initial impact parameter  $h$ , the initial reduced eccentricity  $k$ , and the initial phase  $\varphi$ . A detailed exploration, analogous to what has been done here for the circular case, is clearly not feasible. Petit and Hénon (1986; see also Petit, 1985) have used a Monte Carlo approach, in which  $\varphi$  and  $k$  are chosen at random with appropriate distribution functions. Results for the eccentric case have also been given by Giuli (1968a).

Another natural generalization would be to consider orbits with nonzero inclinations. The equations (8) are easily generalized to this case (Hill, 1878). However, in Hill's coordinates, this again introduces two new parameters: the amplitude and phase of the motion perpendicular to the plane. This brings the total to five parame-

ters. Here again a Monte Carlo approach might be indicated.

#### ACKNOWLEDGMENTS

We thank F. Franklin, C. Marchal, S. Tremaine, and a referee for useful comments.

*Note added in proof.* In our literature search for earlier work on the subject, we overlooked a paper by S. Nishida (1983): Collisional processes of planetesimals with a protoplanet under the gravity of the proto-Sun; *Prog. Theor. Phys.* **70**, 93–105. As in previous papers, the three-body problem equations are used, and the starting values are those of circular orbits. Nevertheless, the results are very similar; compare, for instance, Nishida's Fig. 3 with our Figs. 2 and 3.

#### REFERENCES

- BALBUS, S., AND S. TREMAINE (1985). Private communication.
- BRAHIC, A. (1977). Systems of colliding bodies in a gravitational field. I. Numerical simulation of the standard model. *Astron. Astrophys.* **54**, 895–907.
- DERMOTT, S. F., AND C. D. MURRAY (1981). The dynamics of tadpole and horseshoe orbits. I. Theory. *Icarus* **48**, 1–11.
- DOLE, S. H. (1962). The gravitational concentration of particles in space near the Earth. *Planet. Space Sci.* **9**, 541–553.
- FRANKLIN, F. A., AND G. COLOMBO (1978). On the azimuthal brightness variations of Saturn's rings. *Icarus* **33**, 279–287.
- GIULI, R. T. (1968a). On the rotation of the Earth produced by gravitational accretion of particles. *Icarus* **8**, 301–323.
- GIULI, R. T. (1968b). Gravitational accretion of small masses attracted from large distances as a mechanism for planetary rotation. *Icarus* **9**, 186–190.
- GOLDREICH, P., AND S. TREMAINE (1979). Towards a theory for the Uranian rings. *Nature* **277**, 97–99.
- GOLDREICH, P., AND S. TREMAINE (1980). Disk-satellite interactions. *Astrophys. J.* **241**, 425–441.
- HENON, M. (1969). Numerical exploration of the restricted problem. V. Hill's case: Periodic orbits and their stability. *Astron. Astrophys.* **1**, 223–238.
- HENON, M. (1970). Numerical exploration of the restricted problem. VI. Hill's case: Non-periodic orbits. *Astron. Astrophys.* **9**, 24–36.
- HENON, M. (1981). A simple model of Saturn's rings. *Nature* **293**, 33–35.
- HENON, M. (1984). A simple model of Saturn's rings—revisited. In *Planetary Rings*, Proceedings of the I.A.U. Colloquium No. 75 (A. Brahic, Ed.), pp. 363–382. Cepadues-Editions, Toulouse.
- HENON, M., AND J.-M. PETIT (1986). Series expansions for encounter-type solutions of Hill's problem. To appear in *Celestial Mechanics* (Paper I).
- HILL, G. W. (1878). Researches in the lunar theory. *Am. J. Math.* **1**, 5–26, 129–147, 245–260.
- KARTTUNEN, H. (1983). The wake model for azimuthal brightness variations in Saturn's A-ring. *The Moon and the Planets* **29**, 117–120.
- MARCHAL, C. (1977). Time-asymptotic behavior of solutions of systems of conservative differential equations and of measure-preserving transformations. *J. Differ. Equations* **23**, 387–401.
- PETIT, J.-M. (1985). Simulation numérique des anneaux de Saturne. Thèse de 3e cycle, Université de Nice.
- PETIT, J.-M., AND M. HENON (1986). A numerical simulation of planetary rings. I: Binary encounters. In preparation.
- SCHOFIELD, N. (1981). On the formation of the Earth and Moon by gravitational accretion in a dust disc. *Mon. Not. R. Astr. Soc.* **197**, 1031–1047.
- SPIRIG, F., AND J. WALDVOGEL (1985). The three-body problem with two small masses: a singular-perturbation approach to the problem of Saturn's coorbiting satellites. In *Stability of the Solar System and its Minor Natural and Artificial Bodies*, NATO Advanced Study Institute Series, C (V. Szebehely, Ed.). Reidel, Dordrecht.
- SZEBEHELY, V. (1967). *Theory of Orbits: The Restricted Problem of Three Bodies*. Academic Press, New York.
- YODER, C. F., G. COLOMBO, S. P. SYNNOTT, AND K. A. YODER (1983). Theory of motion of Saturn's coorbiting satellites. *Icarus* **53**, 431–443.